

12  
P.S.

LEVEL III

AD-E300 742

✓DNA 4870F

ADA083452

# DEVELOPMENT OF A PIEZOELECTRIC SHEAR STRESS GAGE FOR DYNAMIC LOADING

Y. M. Gupta  
W. J. Murri  
SRI International  
333 Ravenswood Avenue  
Menlo Park, California 94025

1 December 1978

Final Report for Period June 1978—November 1978

CONTRACT No. DNA 001-78-C-0206

APPROVED FOR PUBLIC RELEASE;  
DISTRIBUTION UNLIMITED.

THIS WORK SPONSORED BY THE DEFENSE NUCLEAR AGENCY  
UNDER RDT&E RMSS CODE B344078462 J11AAXSX35256 H2590D.

FILE COPY

Prepared for  
Director  
DEFENSE NUCLEAR AGENCY  
Washington, D. C. 20305

DTIC  
ELECTE  
S D  
APR 23 1980  
B

80 3 20 002

Destroy this report when it is no longer needed. Do not return to sender.

PLEASE NOTIFY THE DEFENSE NUCLEAR AGENCY,  
ATTN: STTI, WASHINGTON, D.C. 20305, IF  
YOUR ADDRESS IS INCORRECT, IF YOU WISH TO  
BE DELETED FROM THE DISTRIBUTION LIST, OR  
IF THE ADDRESSEE IS NO LONGER EMPLOYED BY  
YOUR ORGANIZATION.





UNCLASSIFIED

SECURITY CLASSIFICATION OF THIS PAGE(When Data Entered)

20. ABSTRACT (Continued)

Impact experiments, using the recently developed combined compression and shear loading facility, were conducted to verify the use of  $163^{\circ}$  Y-cut  $\text{LiNbO}_3$  for shear stress gages. The results of these experiments show that the gage has negligible sensitivity to compressive stresses and a very large sensitivity to shear stresses. Hence,  $163^{\circ}$  Y-cut  $\text{LiNbO}_3$  may be used as a stress gage sensitive only to shear loading.

Further development of gages for routine use in laboratory and field measurements requires additional calibration experiments and development of proper packaging techniques for field experiments.

UNCLASSIFIED

SECURITY CLASSIFICATION OF THIS PAGE(When Data Entered)

## PREFACE

The authors wish to express sincere appreciation to D. D. Keough for many helpful suggestions and discussions during this work. D. Henley, D. Walter, R. Allen, and A. Bartlett also gave valuable technical assistance. Discussions with R. A. Granam of Sandia Laboratories with regard to piezoelectric response under impact loading are gratefully acknowledged. This contract was monitored by Mr. T. Kennedy of the Defense Nuclear Agency.

ACCESSION for	
NTIS	White Section <input checked="" type="checkbox"/>
DDC	Buff Section <input type="checkbox"/>
UNANNOUNCED	<input type="checkbox"/>
JUSTIFICATION _____	
BY _____	
DISTRIBUTION/AVAILABILITY CODES	
Dist.	AVAIL. and/or SPECIAL
A	

CONTENTS

LIST OF ILLUSTRATIONS. . . . .	2
LIST OF TABLES . . . . .	3
ACKNOWLEDGMENTS. . . . .	4
I INTRODUCTION AND SUMMARY. . . . .	5
A. Motivation and Objectives . . . . .	5
B. Background and Approach . . . . .	6
C. Summary . . . . .	8
II THEORETICAL CONSIDERATIONS. . . . .	10
A. Simplifying Assumptions . . . . .	10
B. Elastic Wave Propagation. . . . .	11
C. Piezoelectric Relations . . . . .	13
D. Optimal Gage Design . . . . .	16
III EXPERIMENTAL METHOD AND RESULTS . . . . .	19
A. Experimental Design and Method. . . . .	19
B. Experimental Results. . . . .	23
IV DISCUSSION. . . . .	31
A. Discussion of the Experimental Results. . . . .	31
B. Recommendations for Further Gage Development. . . . .	31
REFERENCES . . . . .	34
APPENDICES	
A: Operation Modes for Piezoelectric Gages. . . . .	37
B: Transformation of Piezoelectric Constants. . . . .	41

ILLUSTRATIONS

1 Schematic View of the Impact Experiment. . . . .	20
2 Photograph of the Projectile and Target Assembly Used in the Impact Experiments . . . . .	22
3 Output from X-cut $\text{LiNbO}_3$ Gages Plotted as a Function of Normalized Time. . . . .	26
4 Results from the $163^\circ$ Y-cut $\text{LiNbO}_3$ Impact Experiment . . .	29

TABLES

1. Experimental Parameters for $\text{LiNbO}_3$ Impact Experiments . . .	24
B-1. Numerical Values of Transformed Piezoelectric Constants ( $\text{C}/\text{m}^2$ ) for $\text{LiNbO}_3$ . . . . .	43

## I INTRODUCTION AND SUMMARY

### A. Motivation and Objectives

The determination of dynamic stresses and loads is fundamental to much of DNA field testing. The need for these measurements has led to the development and use of many different types of stress, particle velocity, acceleration, and displacement gages.<sup>1,2</sup> Despite the large variety and quantity of existing dynamic measurements, field measurements of shear stress (or loads) are lacking. The inability to make dynamic shear measurements is an important shortcoming, because shear measurements are needed for determining strength properties of both soils and structures in underground tests.

The need for shear measurements is well recognized by most workers involved in dynamic measurements. However, this development has been lacking due to the complexity of the problem: The desired shear stress gage must be usable under complex loading conditions, and suitable methods are needed to calibrate the gage to well-defined shear stresses. Most of the previous field gage techniques have been extended from laboratory concepts and measurements, but laboratory studies are also lacking in dynamic shear measurements.

The objective of our work was thus to examine the feasibility of developing a piezoelectric shear stress gage for use in DNA field tests. A combined analytic and laboratory experimental effort was undertaken to meet this objective. The bases for this work are recent developments at SRI relating to the study of dynamic shear properties of solids<sup>3,4</sup> and the use of piezoelectric gages in studying dynamic compressive stresses.<sup>5-9</sup>

## B. Background and Approach

Piezoelectricity and the use of piezoelectric transducers and devices in acoustic applications is a major field of study.<sup>10-12</sup> However, the use of piezoelectric transducers for measuring large stress amplitudes under dynamic loading is a more recent and specialized topic.<sup>13</sup> Studies during the past decade have led to the development of stress transducers for studying dynamic compressive stresses up to tens of kilobars in materials subjected to impact, explosive, and radiation loads.<sup>5-9</sup> Studies by Graham and co-workers have clarified piezoelectric response at high stresses and established bounds on the use of stress gages.<sup>14-16</sup> The formulation of nonlinear piezoelectric constitutive relations has also received increased attention.<sup>15,17</sup> In many laboratory and field measurements, alpha quartz is used as the gage material, but recent studies have also been conducted using lithium niobate ( $\text{LiNbO}_3$ ).<sup>18</sup> For low stresses (below 10 kbar), the larger electrical output of  $\text{LiNbO}_3$  is advantageous.

Piezoelectric gages are used in two modes. The current or short-circuit mode measures fast rise time, i.e., short-duration stress pulses, and the useful recording time of the gage is the wave transit time through the gage. Laboratory shock wave experiments with zero lateral strains commonly use the current mode. In the charge or open-circuit mode, the gage is used to record slower rise time, long-duration (milliseconds) pulses. This second mode is more commonly used under field conditions for recording stress pulses with wavelengths much greater than the gage thickness. That is, the gage in the charge mode acts like a static transducer in equilibrium with the surrounding material stresses. No fundamental differences exist between these modes with regard to the piezoelectric response, and the laboratory results are applicable to field usage. The differences in these modes are operational and reflect the mechanical boundary conditions most suited for using the gages in different applications. Further discussion of these two operational modes is given in Reference 6 and Appendix A.

Despite the many laboratory and field developments in the use of the above-cited modes, measurements to date have been performed exclusively for compressive stresses. In the following paragraphs we discuss our approach for developing a piezoelectric shear stress gage for use in dynamic loading conditions in the presence of complex stresses.

The two general requirements in the development of a shear gage are: (a) knowledge of a material phenomenon (e.g., appropriate piezoelectric response) relating shear stress to a measurable quantity and (b) the ability to calibrate the gage for known shear stresses.

The first requirement is easily satisfied, in principle, because of the existence of many shear transducers in the field of ultrasonics.<sup>11</sup> Because the compressive stress gage is an extension of ultrasonic concepts, these concepts can be explored for the development of a shear stress gage. There are, however, complicating factors that do not allow a simple extension of ultrasonic concepts. In ultrasonics, pure shear waves are commonly created by using the converse piezoelectric effect. Thus, the measuring transducer is subjected to a pure shear motion. In most dynamic loading situations, a complex stress state exists--that is, superposed compression and shear states. Furthermore, because of the large stresses, the material in which the gage is placed undergoes inelastic deformations and the relative magnitudes of the compression and shear stresses are expected to vary over the time range of interest. For the gage measurements to be useful, the electrical signal from the gage should be uniquely related only to the shear stress of interest. Because of the tensorial nature of piezoelectricity, this requirement is not met by most of the ultrasonic shear transducers.

To satisfy the above requirement in the presence of complex stresses (e.g., combined compression and shear), we developed an analytic approach that consists of simultaneously examining wave propagation and piezoelectric relations for materials of interest. The analytic approach chosen is quite general and provides criteria

for determining the needed gage designs. We examine all possible crystal orientations to obtain the optimal directions for piezoelectric response and to determine pure mode directions ('specific directions') for stress wave propagation. Once the optimal gage designs have been analytically evaluated, we can conduct experiments to verify and calibrate these gage designs.

The second requirement, calibration of the gages, is met by experimentally studying the gage response to one-dimensional compression and shear waves using the recently developed IMPS<sup>\*</sup> experimental facility.<sup>4†</sup> In this method, the specimens are subjected to varying but controlled amounts of compression and shear stresses. By subjecting the gages to pure compression, we can ensure that there is no electrical output from the compressive stress. Increased amounts of shear stresses can then be superposed to calibrate the response to shear. Because this is a feasibility study, the present scope of the work is intended to experimentally verify the theoretical concepts. A detailed calibration would be performed after the feasibility of the shear gage has been established.

### C. Summary

The objective of the work reported here was to examine the feasibility of developing a piezoelectric shear stress gage sensitive only to shear loading. Using a combined analytic and experimental approach, we successfully demonstrated the feasibility of developing such a gage.

A simplified but general analysis of the mechanical and piezoelectric response was carried out to provide criteria for a suitable shear gage. Mechanical wave propagation analysis in anisotropic electric media showed that, in general, three waves are propagated: one quasilongitudinal and two quasitransverse waves. Only for 'specific directions' are the propagated waves purely longitudinal and/or purely

\* Internal Measurement of P and S Waves.

† Work performed under DNA Contract DNA001-76-C-0384.

transverse. To avoid mechanical coupling of strains, the gage thickness direction should be along a specific direction. The piezoelectric analysis showed that electrical polarization for the desired gage should be one-dimensional and along the gage thickness direction. Furthermore, this electrical polarization should be caused only by shear loads and not compressive loads.

The adequacy of a particular crystal type for meeting the above criteria can be easily and efficiently assessed by numerical calculations of the specific directions and the 'piezoelectric matrix' for all possible orientations about the three crystallographic axes. When these calculations were carried out for the different orientations of alpha quartz and lithium niobate ( $\text{LiNbO}_3$ ), only the  $163^\circ$  Y-cut  $\text{LiNbO}_3$  appeared suitable for use as a shear gage. For this orientation, the shear-to-compression sensitivity ratio for the polarization is more than two orders of magnitude. Furthermore, this orientation deviates only  $2^\circ$  from a specific direction and therefore has minimal mechanical coupling.

Impact experiments were conducted under combined compression and shear to verify the use of  $163^\circ$  Y-cut  $\text{LiNbO}_3$  as a shear stress gage. The results of these experiments show that the gage, as desired, had negligible sensitivity to compressive stress and a very large sensitivity to shear stress (Section III).

Further development of gages for routine use in laboratory and field measurements requires calibration experiments that can be performed using the same impact facility. In addition, field usage requires development of proper packaging techniques. A brief discussion of these calibration and packaging requirements is also presented in this report (Section IV).

## II THEORETICAL CONSIDERATIONS

This section describes the bases for selecting the gage designs used in our impact experiments. We present the simplifying assumptions made in our analysis, followed by an examination of elastic wave propagation and piezoelectric relations for the materials of interest. Then we describe the specific gage designs selected on the basis of these analytic concepts. The analysis presented here is not conceptually new, but rather is a synthesis of existing studies<sup>5,10,17</sup> for our objectives.

We are primarily concerned with two specific crystals: alpha-quartz and lithium niobate ( $\text{LiNbO}_3$ ). These crystals have been used in previous dynamic measurements because of their high mechanical strength and easy availability.

### A. Simplifying Assumptions

Finite strains and large electric fields are created in the piezoelectric gages subjected to large amplitude stress waves. Thus, a detailed discussion of the piezoelectric constitutive relations should incorporate finite strain effects, electromechanical coupling, and changes in dielectric permittivity.<sup>15</sup> Analysis of the experimental results should also consider these nonlinear effects,<sup>17,18</sup> but such an effort is beyond the scope of a feasibility study.

In the present work, we make use of two simplifying assumptions: "linearity" and "no coupling."<sup>17</sup> The first assumption gives a linear stress-strain relation and a linear piezoelectric relation. The second assumption permits us to neglect the effect of electric fields on mechanical variables such as strains and wave velocities. Therefore, we can study the piezoelectric response in two separate parts: elastic wave propagation (mechanical loading) and piezoelectric relations. Each of these two parts suggest desirable features for the gage design.

## B. Elastic Wave Propagation

Wave propagation in a linear elastic anisotropic medium has been the subject of considerable work in ultrasonics and acoustics.<sup>19-21</sup> Johnson has applied these concepts to planar impact problems and has obtained analytic solutions that show multiple wave structure because of crystalline anisotropy.<sup>22</sup> Below, we summarize the main features of elastic wave propagation in anisotropic crystals.\*

We consider two coordinate systems:<sup>22</sup>  $x_i$  corresponds to the crystallographic system and  $x'_i$  corresponds to the wave propagation system. Wave propagation is described by<sup>20</sup>

$$\rho \frac{\partial^2 u'_i}{\partial t^2} = C'_{ijkl} \frac{\partial^2 u'_k}{\partial x'_j \partial x'_l} \quad (1)$$

where  $\rho$  = density

$u'_i$  = material displacement along the  $x'_i$ -direction

$t$  = time

$C'_{ijkl}$  = second-order elastic constants in the primed system.

The transformation matrix between the unprimed and primed system is given by

$$a_{mn} = \vec{i}'_m \cdot \vec{i}_n \quad (2)$$

where  $\vec{i}'_m$  and  $\vec{i}_n$  are unit vectors along the  $x'_m$  and  $x_n$  directions.

Plane wave solutions for wave propagation along a direction  $\vec{b}'$  for Equation (1) are given by

$$u'_i = U'_i f(t - b'_n x'_n / c') \quad (3)$$

where  $U'_i$  = displacement amplitude along  $x'_i$

$c'$  = wave velocity.

Substitution of (3) in (1) gives the following equations

---

\* The Einstein summation convention is adopted throughout this report.

$$\left( \lambda'_{ik} - \delta_{ik} \rho c^{-2} \right) U'_k = 0 \quad (4)$$

$$\text{where } \lambda'_{ik} = b'_j b'_\ell C'_{ijkl} \quad (5)$$

For nontrivial solutions of Eq. (4), we have the condition

$$|\lambda'_{ik} - \delta_{ik} \rho c^{-2}| = 0 \quad (6)$$

Equation (6) has three possible eigenvalues, each of which corresponds to an eigenvector  $U'_m$ . Each of the eigenvalues and eigenvectors represent the wave velocity and displacement amplitude associated with one of the three waves. These displacements are always mutually orthogonal but can have an arbitrary orientation with respect to the wave propagation direction  $\vec{b}'$ . Only for specific directions (or isotropic materials) are the displacement directions either parallel (longitudinal waves) or perpendicular (shear waves) to the direction of wave propagation.<sup>19</sup> In general, there is one quasilongitudinal wave and two quasitransverse waves.

In our experiments we are subjecting the gage to externally applied compressive and shear stresses. If the gage output is to be related to a particular stress component (shear stress in the present case), then no coupling of the stresses should occur within the gage. For the linear elastic behavior considered here, this coupling can arise only because of the crystal anisotropy. Therefore, the crystals used for gage development should be oriented along the specific directions\* for the compressive and shear wave of interest in our experiments.

The specific directions for a particular crystal depend on the symmetry of that crystal class.<sup>†</sup> Borgnis<sup>19</sup> and Brugger<sup>21</sup> have performed extensive calculations of specific directions for various crystal classes. Because in practical applications small deviations from specific directions can be tolerated, we have chosen to examine wave

\* Specific directions can vary depending on the wave motion of interest (the longitudinal or either of the transverse waves).

† Both  $\text{LiNbO}_3$  and quartz are trigonal crystals.

propagation for quartz and  $\text{LiNbO}_3$  more generally. This is best done by solving Eq. (6) to give the eigenvalues and eigenvectors for each one degree of rotation in the XY, YZ, and ZX planes about the Z, X, and Y axes, respectively. We have numerically carried out this calculation for the YZ plane (rotation about X axis) and the results are discussed in Section II.D. The calculations for XY and ZX planes were not performed because of piezoelectric considerations discussed in the next two subsections.

### C. Piezoelectric Relations\*

The direct piezoelectric effect for the linear approximations made in our work may be expressed as<sup>10</sup>

$$P'_i = e'_{ijk} \epsilon'_{jk} \quad (7)$$

where  $P'_i$  = electrical polarization along  $x'_i$   
 $e'_{ijk}$  = piezoelectric stress coefficient tensor in the primed system  
 $\epsilon'_{jk}$  = strain coefficients in the primed system.

For convenience in our impact experiments, we have chosen to express the piezoelectric effect in terms of mechanical strains instead of stresses. On the other hand, for the field measurements, it is convenient to express the polarization in terms of the stresses.

$$P'_i = d'_{imn} \sigma'_{mn} \quad (8)$$

where  $d'_{imn}$  = piezoelectric strain coefficient tensor in the primed system  
 $\sigma'_{mn}$  = stresses in the primed system.

Using Hooke's Law, we can express the relationship between the d's and e's as

$$e'_{ijk} = d'_{ipq} C'_{pqjk} \quad (9)$$

---

\* We are ignoring pyroelectric effects in our discussion.

Equations (7) and (8) are equivalent representations, and the use of either form is a matter of convenience based on the mechanical boundary conditions.

Equation (7) can be expressed in matrix notation as<sup>10</sup>

$$\begin{pmatrix} P_1' \\ P_2' \\ P_3' \end{pmatrix} = \begin{pmatrix} e_{11}' & e_{12}' & e_{13}' & e_{14}' & e_{15}' & e_{16}' \\ e_{21}' & e_{22}' & e_{23}' & e_{24}' & e_{25}' & e_{26}' \\ e_{31}' & e_{32}' & e_{33}' & e_{34}' & e_{35}' & e_{36}' \end{pmatrix} \begin{pmatrix} \epsilon_1' \\ \epsilon_2' \\ \epsilon_3' \\ \epsilon_4' \\ \epsilon_5' \\ \epsilon_6' \end{pmatrix} \quad (10)$$

where we have replaced the strain matrix  $\epsilon_{jk}'$  by the column vector  $\epsilon_n'$ , and the off diagonal elements of  $\epsilon_{jk}'$  are given by  $n > 3$ . For the desired gage, we have the following requirements: (1)  $P_i'$  should have only one component, (2) this component should be produced only by a shear strain\*  $\epsilon_n'$  (where  $n > 3$ ), and (3) the component should be parallel to the gage thickness direction.

We now examine the piezoelectric response for the loading situation present in our impact experiments. Let  $X_2'$  be the direction through the gage thickness and  $\epsilon_2'$  and  $\epsilon_4'$  be the non-zero strains. Calculation of polarization  $P_2'$  solely caused by  $\epsilon_4'$  requires that the piezoelectric matrix  $e_{ij}'$  in Equation (10) possess a particular form. To determine the adequacy of alpha quartz (crystal class 32) and  $\text{LiNbO}_3$  (crystal class 3m) for our purposes, we first write down the piezoelectric tensor in the crystallographic system ( $X_i$  system)<sup>10</sup>

$$\text{Quartz:} \quad \begin{pmatrix} e_{11} & -e_{11} & 0 & e_{14} & 0 & 0 \\ 0 & 0 & 0 & 0 & -e_{14} & -e_{11} \\ 0 & 0 & 0 & 0 & 0 & 0 \end{pmatrix} \quad (11)$$

\* Because the gage behaves elastically, either stresses or strains can be used in the discussion.

$$\text{LiNbO}_3: \begin{pmatrix} 0 & 0 & 0 & 0 & e_{15} & -2e_{22} \\ -e_{22} & e_{22} & 0 & e_{15} & 0 & 0 \\ e_{31} & e_{31} & e_{33} & 0 & 0 & 0 \end{pmatrix} \quad (12)$$

Of the three directions in the crystallographic system ( $X_i$  system), only Y-cut quartz and X-cut and Y-cut  $\text{LiNbO}_3$  will give non-zero polarization for applied shear strains. Therefore, we have the following situation for combined compression and shear loading (present in our experiments) for these orientations:

$$\begin{aligned} \text{Y-cut quartz:} & \quad P_1 \neq 0, P_2 \neq 0 \\ & (\epsilon_2 \neq 0, \epsilon_6 \neq 0) \end{aligned}$$

$$\begin{aligned} \text{X-cut LiNbO}_3: & \quad P_1 \neq 0, P_2 \neq 0, P_3 \neq 0 \\ & (\epsilon_1 \neq 0, \epsilon_6 \neq 0) \end{aligned}$$

$$\begin{aligned} \text{Y-cut LiNbO}_3: & \quad P_1 \neq 0, P_2 \neq 0, P_3 \neq 0 \\ & (\epsilon_2 \neq 0, \epsilon_4 \neq 0) \end{aligned}$$

In the presence of pure shear strains (as is often the case in ultrasonic applications), the above orientations are satisfactory because only one polarization term will be non-zero. However, in the presence of compressive loading, these orientations give rise to unwanted polarizations. Thus, for complex loading situations we must include the effect of additional polarization fields and not just the polarization field for shear.<sup>2,11,12</sup> A possible method to minimize the effect of these unwanted polarization fields is discussed in the next subsection.

A fundamental method of eliminating the undesired polarization fields is to find a suitable crystal orientation such that the piezoelectric tensor has the desired form--that is, where the polarization field is one-dimensional and is caused solely by shear loads. The transformation for the piezoelectric tensor is expressed as

$$e'_{ijk} = a_{il} a_{jm} a_{kn} e_{lmn} \quad (13)$$

An efficient way to determine the crystal directions of interest is to numerically transform the tensor  $e_{\lambda mn}$  for each one-degree rotation in the XY-plane (rotation about the Z-axis), the YZ-plane (rotation about the X-axis), and the ZX-plane (rotation about the Y-axis). By expressing the transformed piezoelectric constants in a matrix notation similar to that of Equation (11) or (12), we can quickly scan through the results and determine the desired orientation. The numerical method and results are presented in Appendix B. We have used this method to examine the piezoelectric tensor for alpha quartz and  $\text{LiNbO}_3$ , and the results of these calculations are discussed below.

#### D. Optimal Gage Design

The development of an optimal gage design has three requirements based on theoretical considerations: (a) the electric polarization must be due to shear stress (or strain) in the gage, (b) the polarization must be one-dimensional and along the gage thickness direction and, (c) the gage thickness direction must be a specific direction. We have examined alpha quartz and  $\text{LiNbO}_3$  in terms of these requirements. Appendix B presents the results of the transformed piezoelectric matrices for rotation about the X-axis for  $\text{LiNbO}_3$ . The transformed matrices for quartz and the other two axes in  $\text{LiNbO}_3$ , and calculations of specific direction, have also been carried out but are not presented here.

In alpha quartz it is not possible to eliminate the unwanted polarizations by using a rotated crystal cut. The possibility of mitigating the effects of such polarizations by suitable circuit design is considered later in our discussion on  $\text{LiNbO}_3$ .

The results of the calculation for  $\text{LiNbO}_3$  show that the  $163^\circ$  Y-cut is the optimal direction from polarization considerations.\* The numerical values of the piezoelectric matrix ( $e'_{ij}$ ) for this orientation expressed in the units of Coulomb/m<sup>2</sup> are:

---

\*  $163^\circ$  Y-cut implies a  $163^\circ$  rotation about the X-axis. See Institute of Radio Engineers (IRE) convention (Reference 23).

$$e'_{ij} = \begin{pmatrix} 0 & 0 & 0 & 0 & -2.9 & 3.4 \\ 2.39 & -8 \times 10^{-3} & -1.72 & -3.76 & 0 & 0 \\ .49 & -.38 & -2.27 & -.69 & 0 & 0 \end{pmatrix} \quad (14)$$

The transformed values show that for  $\epsilon'_2 \neq 0$  and  $\epsilon'_4 \neq 0$  (the condition of interest in our impact experiments), the shear contribution to  $P'_2$  is more than two orders of magnitude larger than the compressive contribution. Although  $P'_1$  is zero, for this orientation, the value of  $P'_3$ , although small, is not completely negligible. The need to ascertain the influence of  $P'_3$  is discussed in Section IV.

The results presented in Appendix B show the marked sensitivity of the piezoelectric tensor to small changes in the angles. Both the  $162^\circ$  and  $164^\circ$  Y-cut directions have lower shear-to-compression sensitivity ratios in comparison to the  $163^\circ$  angle. These results emphasize the need for accurate knowledge of the piezoelectric constants ( $e_{ijk}$  in the crystallographic system) and for precise crystal orientation in gage fabrication.

The  $163^\circ$  Y-cut direction is also a desirable orientation on the basis of the mechanical considerations. We have computed the eigenvalues and eigenvectors of Equation (6) for all directions in the Y-Z plane, using constant electric displacement elastic constants.<sup>24</sup> These calculations show that the  $165^\circ$  Y-cut orientation is a specific direction. Also, the longitudinal particle motion direction for wave propagation along the  $163^\circ$  Y-cut orientation is along  $161.7^\circ$ , and hence the mechanical coupling effects due to crystal anisotropy are quite minimal. The complete set of eigenvectors for the  $163^\circ$  orientation is: (1, 0, 0), (0, -0.949, 0.3145), and (0, 0.3145, 0.949).

The use of  $163^\circ$  Y-cut  $\text{LiNbO}_3$  for acoustic applications has been proposed by Warner, et al.<sup>24</sup> However, the criteria derived in our work are more general\* and can be used to evaluate any crystal for use as a shear stress gage under dynamic loading.

\*For example, our analysis shows that alpha quartz is not suitable as a shear gage.

These analytic considerations show that even the optimal gage direction for shear response is not ideal, as is frequently the case for compressive stress gages. Further discussion of the departures from ideal considerations is given in Section V.

We also conducted experiments on X-cut  $\text{LiNbO}_3$ , because, some X-cut crystals were immediately available and because we wanted to examine a possible method of minimizing the effect of the unwanted polarizations. We wanted to find out whether the 'shorted' gage configuration (the gage sides are also plated) would aid in minimizing the effects of the unwanted polarization.

### III EXPERIMENTAL METHOD AND RESULTS

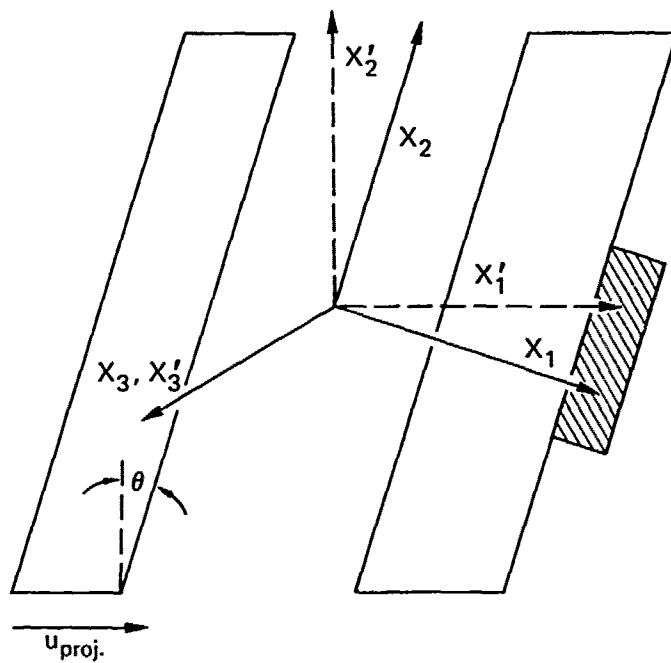
The gage designs determined from theoretical considerations were experimentally checked by performing impact experiments under combined compression and shear loading. This section describes the gage fabrication, experimental techniques used, and the results of these impact experiments.

#### A. Experimental Design and Method

All of the  $\text{LiNbO}_3$  gages used in our work were fabricated by Specialty Engineering Associates according to our specifications. The  $\text{LiNbO}_3$  crystals were cut to the desired orientation (within one degree).<sup>\*</sup> The flatness and parallelism requirements were typical of piezoelectric gages used in impact experiments. All the gages were gold-plated on all sides (i.e., wrap around or shorted configuration). Guard rings were cut on the back side and a 50-ohm resistor was shunted across the guard ring. The gages were built into an aluminum housing with epoxy potting at the rear of the gage. These gages were designed to record useful information for one-wave transit time through the gage. The guard-ring and gage dimensions were similar to those used in studies on compressive stress gages.<sup>5-8</sup>

All the experiments performed in this work employed the back surface gage configuration shown in Figure 1. A flyer plate inclined at an angle  $90^\circ - \theta$  to the axis of the projectile motion impacts a parallel specimen plate backed by the piezoelectric gage. The shear axis on the gage plane has to be accurately aligned to the direction of shear stress imparted by the projectile impact. Upon impact, two waves are propagated into the flyer and specimen: a compressive and a shear wave. The compressive wave, which travels at a faster velocity, impacts the gage, resulting in a transmitted wave into the

\* Future gages will be fabricated with tolerances to within  $\pm 1/2^\circ$ .



MA-7306-1

FIGURE 1 SCHEMATIC VIEW OF THE IMPACT EXPERIMENT

The piezoelectric shear stress gage is bonded to the rear surface of the specimen. Note, that  $X_1$  is normal to the gage and  $X_2$  is parallel to the shear direction in the gage.

gauge and a reflected wave in the specimen. The slower traveling shear wave interacts with the reflected compressive wave<sup>\*</sup> and arrives at the specimen-gauge interface. For a gauge responding only to shear, we expect to see no signal from the compressive wave and a large signal after the arrival of the shear wave.

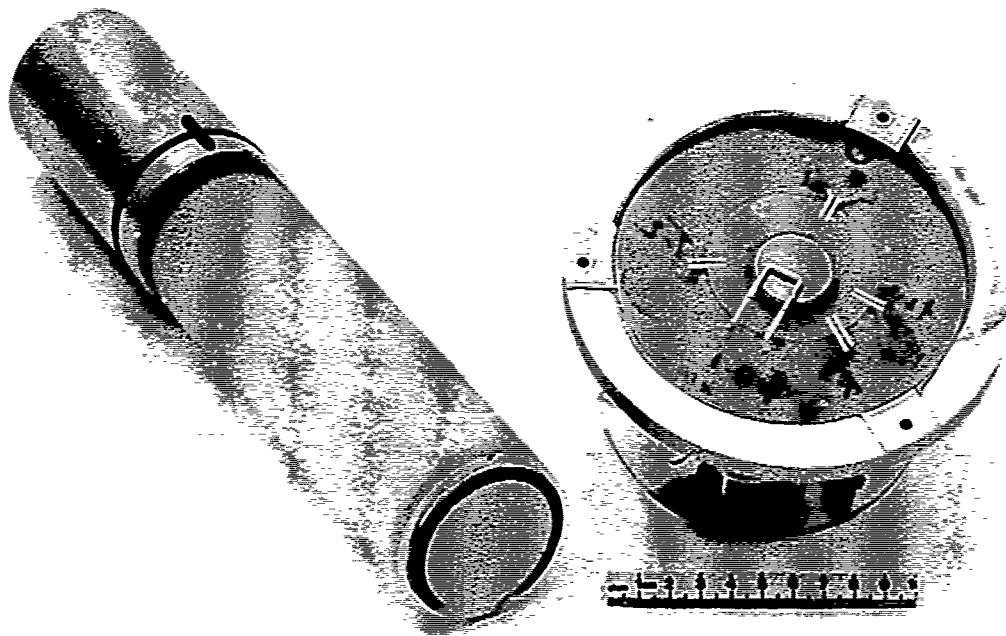
The use of a back surface gauge for determining gauge calibrations is complicated because it is necessary to have accurate knowledge of the shear response of the specimen, the wave interactions in the specimen, and the shear strength of specimen-gauge interface. However, the accurate determination of gauge calibration was not the objective of this study. Instead, we intended only to examine the experimental feasibility of the theoretically determined gauge designs. The back surface gauge configuration, because of the temporal separation between the compressive and shear waves, permits an efficient assessment in a single experiment of the desired gauge features: no signal from the compressive wave and a large signal from the shear wave. In future experiments for determining quantitative calibrations, we will use the impact surface gauge configuration.<sup>26</sup>

The impact experiments were performed using the SRI gas-gun facility for studying one-dimensional compression and shear wave propagation in solids. Details of the gun-barrel, target holder, and related instrumentation for measuring projectile velocity and impact misalignment are given in Reference 4. Seven experiments were performed: two experiments with X-cut  $\text{LiNbO}_3$  gauges and five with  $163^\circ$  Y-cut  $\text{LiNbO}_3$  gauges. The  $\text{LiNbO}_3$  gauges were bonded to the specimen plates (Polymethyl-methacrylate discs) using epoxy resin (Epon 815 and hardener<sup>†</sup>). The specimen-gauge assemblies were potted in aluminum target rings as shown in Figure 2. In some experiments, front surface particle velocity gauges were vapour-deposited on the PMMA specimen

---

\* In our present work, we assume linearity and have ignored this interaction.

† Shell Co.



MP-7306-2

**FIGURE 2** PHOTOGRAPH OF THE PROJECTILE AND TARGET ASSEMBLY USED IN THE IMPACT EXPERIMENTS

The Vapor-deposited metallic coating on the projectile shorts the vapor-deposited tilt pins on the target to provide a measurement of the impact alignment.

discs to record the particle velocities imparted to the specimens. Tilt pins were vapour-deposited, and trigger foils were bonded to all the specimens as shown in Figure 2. The flyer plates for the two X-cut  $\text{LiNbO}_3$  and the three  $163^\circ$  Y-cut  $\text{LiNbO}_3$  experiments were PMMA discs. The remaining two experiments used flyer plates made from syntactic foam ECCO float EF-38.\* The rationale for using the foam flyer plates is discussed in the next section.

### B. Experimental Results

Table I summarizes the experimental details from the seven impact experiments conducted. The first nine columns are self-explanatory. The longitudinal compressive stresses cited in the last column are the stresses in the  $\text{LiNbO}_3$  gage based on a linear elastic calculation:

$$\sigma_g^L = \frac{2Z_g^L}{Z_g^L + Z_p^L} \sigma_p^L \quad (15)$$

where

$\sigma_g^L$  = Longitudinal stress in the gage

$Z_g^L$  = Longitudinal mechanical impedance of the gage (function of crystal orientation)

$Z_p^L$  = Longitudinal mechanical impedance of PMMA specimen

$\sigma_p^L$  = Longitudinal stress caused by the impact in PMMA

The longitudinal particle velocities in the PMMA are either measured or known from the symmetric impact conditions. These velocities in turn permit a determination of  $Z_p^L$  and  $\sigma_p^L$  using the data of Barker and Hollenbach.<sup>27</sup> The mechanical impedance of the  $\text{LiNbO}_3$  ( $Z_g^L$ ) is known from the wave velocity calculations outlined in the last section.

\* Trademark, Emerson and Cuming Inc., Floatation Products Division, Canton, Mass.

Table I  
EXPERIMENTAL PARAMETERS FOR  $\text{LiNbO}_3$  IMPACT EXPERIMENTS

Experiment Number	Gage Type	Gage Thickness (mm)	Active Electrode Diameter (mm)	Flyer Plate Material	Impact Velocity (mm/ $\mu$ s)	Impact Angle (degrees)	Tilt <sup>a</sup> ( $\mu$ s)	PMMA Specimen Thickness (mm)	Long. Stress in $\text{LiNbO}_3$ (kbar)
1 (78-2-22)	X-cut	2.4	8	PMMA	0.158	0°	0.4	0.737	5.1
2 (78-2-23)	X-cut	2.4	8	PMMA	0.159	10°	0.5	0.645	5.0
3 (78-2-31)	163° Y-cut	5.0	4	PMMA	0.155	0°	0.6	1.173	5.0
4 (78-2-32)	163° Y-cut	5.0	4	PMMA	0.160	10°	1.2	1.0	5.1
5 (78-2-36)	163° Y-cut	5.0	4	FOAM	0.259	0°	0.27	3.78	1.75
6 (78-2-37)	163° Y-cut	5.0	4	FOAM	0.263	10°	0.1	1.78	0.9
7 (78-2-46)	163° Y-cut	5.0	4	PMMA	0.2	20°	0.36	1.41	6.0

<sup>a</sup> As defined by closure time over a 52-mm-diameter circle.

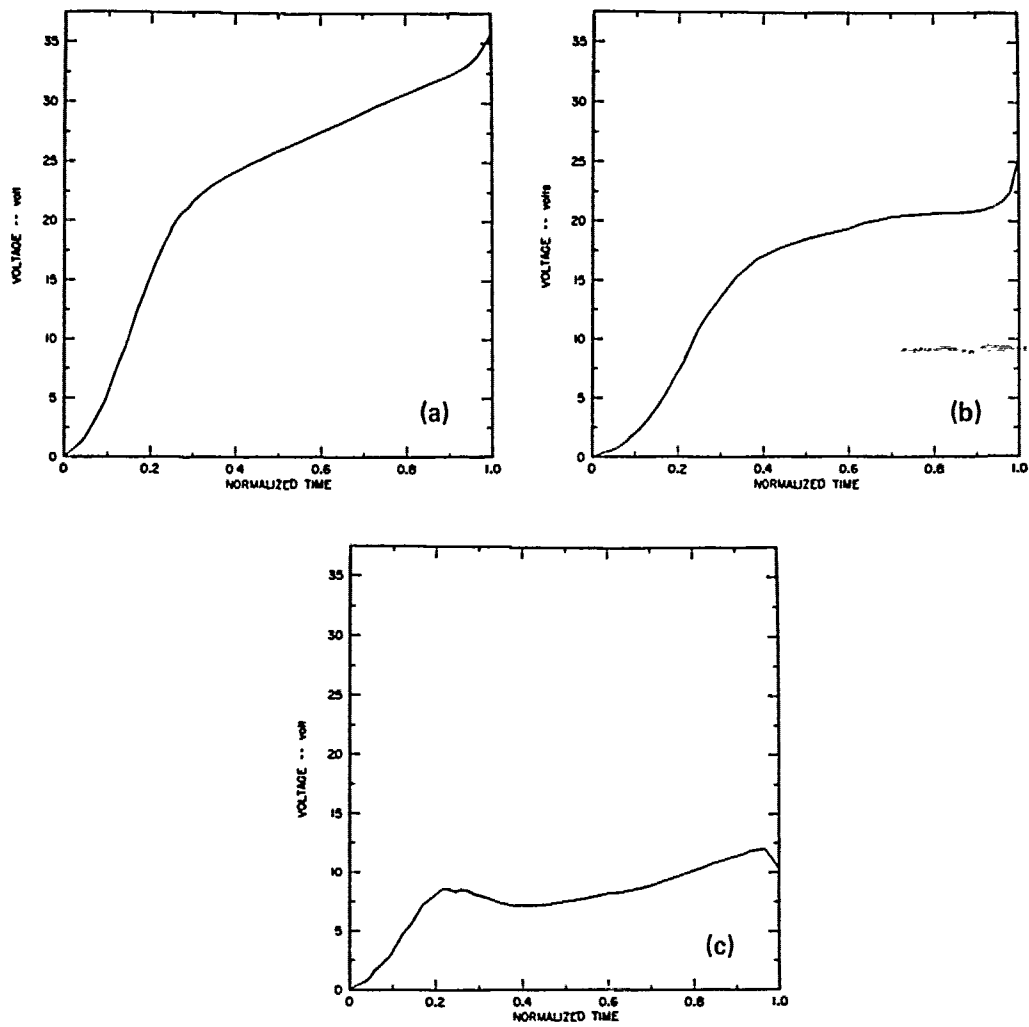
The first series of experiments were conducted on X-cut  $\text{LiNbO}_3$ . The gage dimensions used were the sizes that were readily available. The first shot was a uniaxial strain shot to determine the effect of the shorting configuration in reducing the polarization charges perpendicular to the direction of interest. Figure 3(a) shows the voltage-time profile from the shot normalized with respect to the transit time of the signal through the gage. The observed signal is very large and clearly demonstrates the inability of the shorting configuration to eliminate the unwanted polarization charges.

A second X-cut  $\text{LiNbO}_3$  shot was performed with the same compressive stress as the first shot but with a superposed shear stress. The voltage-time profile from this shot is shown in Figure 3(b). An algebraic difference between these two shots is shown in Figure 3(c). This difference can be attributed to shear loading. Although the signal in Figure 3(c) is quite large (approximately 10 volts), no quantitative interpretation of these results is attempted here. The presence of  $P_2'$  and  $P_3'$  polarization terms do not permit the use of assumptions needed to derive the current-stress relationship for the piezoelectric gage.

The results of the X-cut  $\text{LiNbO}_3$  shots show that there is a large sensitivity to shear stress; however, there is also a large sensitivity to compressive stress, despite the shorting configuration, that renders this gage unusable under complex loading conditions.

The remaining five experiments were conducted on  $163^\circ$  Y-cut  $\text{LiNbO}_3$  crystals. These gages were fabricated to our specifications and were 5 mm thick. The use of thicker gages allows the use of thicker PMMA specimens, thereby permitting a larger temporal separation between the compressive and shear wave.

The results of shots 3 and 4 demonstrated a very small output from the compressive wave; however, these results were difficult to interpret because of large impact tilts. The impact tilt gives rise to the following complexities: the large ratio of the wave velocity in  $\text{LiNbO}_3$  to the projectile velocity results in a large inclination of the wavefront and an additional shear wave can be generated. These



MA-7306-3

FIGURE 3 OUTPUT FROM X-CUT  $\text{LiNbO}_3$  GAGES PLOTTED AS A FUNCTION OF NORMALIZED TIME  
 (a) Compression only, Shot #1, (b) Compression and Shear, Shot #2, (c) Difference of Shot #1 and #2 to show signal due to shear. The time has been normalized with respect to transit time through the gage.

effects and the lack of a perfect specific direction for the  $163^\circ$  Y-cut  $\text{LiNbO}_3$  give rise to a complex wave structure. Rather than analyze this wave-structure (using the analysis in Section II.B), we chose to eliminate the problem of large tilts.

A foam flyer plate was used in shots 5 and 6 to permit a higher projectile velocity, thereby reducing the closure time at the impact surface. Particle velocity gages were vapour-deposited on the Lucite specimen plates to determine the input stresses in the Lucite. Shot 5 resulted in a 1.75-kbar compressive pulse, and a negligible signal output from the gage was observed. In shot 6, a combined compressive and shear experiment, the shear particle velocity at the impact surface was measured. Although the signal from the compressive stress was again negligible, the shot was of little value because the foam imparted negligible shear motion to the Lucite specimen.

In shot 7 we used a Lucite flyer, a higher projectile velocity, and a larger angle ( $20^\circ$ ) to cause larger compressive and shear stresses in the PMMA and hence in the  $\text{LiNbO}_3$  gage. An assumed linear elastic response in compression and shear for the PMMA results in a compressive stress of 6 kbar and a shear stress of 1 kbar, respectively, in the  $\text{LiNbO}_3$  gage. However, our work on PMMA\* shows this assumption to be wrong, and therefore the amplitude of the shear wave in PMMA is expected to be considerably smaller than that calculated from the following linear elastic relation

$$\tau = \rho_0 C_p^s u_p^s \quad (16)$$

where  $C_p^s$  = shear wave velocity  
 $u_p^s$  = shear particle velocity in PMMA at the impact surface.

\* We are currently determining the shear stress-strain relation in PMMA under a separate contract with the U.S. Army Research Office.

Figure 4 shows the voltage-time results from shot 7 as recorded on a dual-beam oscilloscope. The upper trace is the  $\text{LiNbO}_3$  gage output and the lower trace is the shear particle velocity profile from the particle velocity gage at the impact surface. The time settings are  $0.2 \mu\text{s}/\text{cm}$  for both traces; the voltage settings are  $1 \text{ V}/\text{cm}$  for the upper trace and  $0.05 \text{ V}/\text{cm}$  for the lower trace.

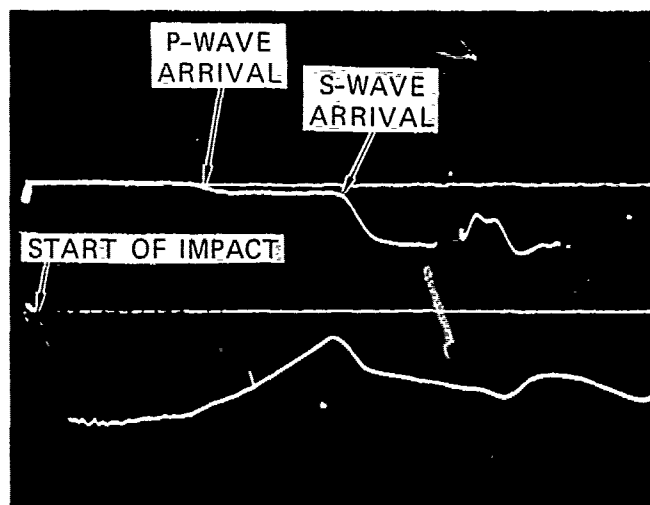
The particle velocity profile at the impact surface (lower trace) shows that initial particle velocity imparted to the specimen is 90% of the value calculated by assuming a "no slip" condition at impact. Only the first  $0.8 \mu\text{s}$  of the signal is useful because of edge rarefactions that influence the gage leads. The decay in the particle velocity  $0.46 \mu\text{s}$  after impact is caused by the shear behavior of PMMA. This decay and other observations suggest that PMMA does not behave in a linear elastic manner, and the  $\text{LiNbO}_3$  gage output from shear is expected to be much smaller than the value expected for a 1-kbar shear stress.

The upper trace shows a small signal output from the  $\text{LiNbO}_3$  gage at the time of the compressive wave arrival at the gage. The compressive wave velocity in PMMA calculated from Figure 3 is in excellent agreement with independent measurements in PMMA made at SRI and elsewhere.<sup>27</sup> The amplitude of the signal from the compressive wave is of the order expected from the small piezoelectric coefficient along the  $163^\circ$  Y-cut direction. In future work, we will make precise comparisons between the theoretically computed values and the experiment results.

The larger signal in the upper trace coincides with the shear wave arrival<sup>\*</sup> at the  $\text{LiNbO}_3$  gage. This result thus shows that the  $163^\circ$  Y-cut  $\text{LiNbO}_3$  can indeed be used to measure the shear stress at the specimen-gage interface. As explained previously, a quantitative comparison of the predicted and measured gage signal is not possible at present because of lack of knowledge of the dynamic shear strain

---

\* Shear wave velocity in PMMA has been determined from other independent measurements.



MP-7306-4

FIGURE 4 RESULTS FROM THE 163° Y-CUT  $\text{LiNbO}_3$  IMPACT EXPERIMENT

The top trace represents output from the  $\text{LiNbO}_3$  gage (1 V/div). The bottom trace represents transverse particle velocity imparted to the PMMA (0.05 V/div). Time scale is common to both traces (0.2  $\mu\text{sec/div}$ ).

behavior of PMMA and the epoxy bond. The decrease in signal  $0.3 \mu\text{s}$  after the arrival of the shear wave coincides with the compressive wave arriving at the back of the gage and represents the limit of useful recording by the gage in our experiment.

The results from the  $163^\circ$  Y-cut  $\text{LiNbO}_3$  experiments may be summarized as follows: these gages demonstrate a very low response to compressive stresses and a large response to shear stresses under dynamic loading conditions. The signal from the shear wave is nearly an order of magnitude higher than the compressive signal. However, the amplitude of the compressive wave is more than an order of magnitude higher than the shear wave amplitude. These results confirm our theoretical calculations. A quantitative calibration of the gages requires additional experiments, as outlined in the next section.

## IV DISCUSSIONS

This section presents a discussion of the theory and the experimental results, as well as specific questions that need to be answered for the development of a gage that can be used routinely in laboratory and field experiments.

### A. Discussion of the Experimental Results

The results of the two experiments on X-cut  $\text{LiNbO}_3$  clearly demonstrated that shear sensitivity of the crystal alone is not a sufficient requirement for developing a gage for use under complex loading situations. Hence, most of the shear transducers commonly used in ultrasonics cannot be used for our purposes.

A fairly general analysis of alpha quartz and  $\text{LiNbO}_3$  provided only one useful gage type:  $163^\circ$  Y-cut  $\text{LiNbO}_3$ , which satisfies almost all the criteria presented in Section II.D. The shear-to-compressive sensitivity ratio has a value of 250.<sup>28</sup> Although our experiments did not provide a complete quantitative check, they did demonstrate the large shear-to-compressive sensitivity ratio. A quantitative comparison of the observed signal with the theoretical calculations can be made using the relation between current and stress given in Appendix A. In future work we will carry out these quantitative comparisons. Furthermore, in future analysis of the experimental results, we need to consider the effect of the small deviation of the  $163^\circ$  direction from a specific direction.

### B. Recommendations for Further Gage Development

We have successfully demonstrated the feasibility of developing a piezoelectric shear stress gage. However, the routine use of a gage for laboratory and field applications requires further assessment of gage response accuracy, quantitative calibration, and proper packaging (for field use). These considerations are briefly discussed below.

The primary requirement for gage development was the determination of the appropriate orientation. The orientation calculations were based on the values of the piezoelectric constants. For  $\text{LiNbO}_3$ , differences in the constants have been reported in the literature.<sup>18</sup> The probable cause of this variation is the material source. By performing a few experiments along a specific direction ( $165^\circ$  Y-cut), we can establish the accuracy of the constants without introducing the complexity caused by the deviation from specific direction. The results of these experiments will provide accuracy bounds for gage calibrations.

In using the piezoelectric tensor (Eq. 14 in Section II.D), we need to examine two other calibration-related questions: (a) What is the effect of  $P_3' \neq 0$  on the gage response? This arises because  $e_{34}'$  is not zero in Equation (14). (b) What is the effect of shear component  $\epsilon_6'$  being non-zero when we are trying to measure the response due to  $\epsilon_4'$  ( $\neq 0$ )? The second question is important in field conditions when an arbitrary shear strain may be present on the gage face. The presence of  $\epsilon_6'$  can give rise to  $P_1' \neq 0$ .

The first question can be answered by conducting precise calibration experiments that would also establish the accuracy of the gage response. The second question can be answered by performing experiments on gages that are rotated  $90^\circ$  with respect to gages used in our work, that is,  $\epsilon_6' \neq 0$  and  $\epsilon_4' = 0$  (Note,  $\epsilon_2'$  is unchanged).

Packaging requirements also need to be addressed for field usage of the gage. Our examination of field work shows that measurements of shear stresses at soil-structure interfaces appear to be most appropriate with the piezoelectric shear stress gage. For packaging, we must consider optimal placement of gages, survivability, and techniques for attaching leads to the electrodes. For field usage, the gage constants are best expressed in terms of the  $d_{ijk}'$ 's and care must be taken to ensure the proper stress boundary conditions (lateral stresses should be zero).

Finally, in future work, we should also examine other candidate materials. Although quartz and Lithium Niobate have been most

extensively studied for large amplitude stress measurements, other materials may better satisfy the criteria outlined in Section II.D for a shear stress gage.

## REFERENCES

1. P. L. Flanders, "Test Sites and Instrumentation," Nuclear Geoplosics, Part III, DNA Report, DASA - 1285 (1964).
2. P. L. Coleman, et al., "Review and Development of Ground Motion and Airblast Instrumentation," DNA 4036F (1976).
3. Y. M. Gupta, Appl. Phys. Letters 29, 694 (1976).
4. Y. M. Gupta, "Development of a Method for Determining Dynamic Shear Properties," Draft Final Report submitted to DNA under Contract DNA 001-76-C-0384 (May 1978).
5. R. A. Graham, F. W. Nielson, and W. B. Benedick, J. Appl. Phys. 36, 1775 (1965); R. A. Graham and R. D. Jacobsen, Appl. Phys. Letters 23, 584 (1973).
6. R. A. Graham, "Lithium Niobate Stress Transducers," in Sandia Technology, Sandia Laboratories Report SAND75-0426 (1975).
7. R. P. Reed, "The Sandia Field Test Quartz Gage, Its characteristics and Data Reduction," Sandia Laboratories Report SC-CD-71-4529 (1971).
8. D. B. Hayes and Y. M. Gupta, Rev. Sci. Instr. 45, 1554 (1974).
9. D. R. Grine, "Hardened Quartz Gages for Ground Shock and Airblast Measurements," Presentation at DNA meeting, Vicksburg, Mississippi (October 1975).
10. W. G. Cady, Piezoelectricity (McGraw-Hill, New York, 1946).
11. W. P. Mason, Piezoelectric Crystals and Their Applications to Ultrasonics (D. Van Nostrand Company, New York, 1950).
12. D. A. Berlincourt, D. R. Curran, and H. Jaffe, in Physical Acoustics, Vol. I (A), Ed. W. P. Mason (Academic Press, New York, 1964); also see articles in subsequent volumes.
13. F. W. Neilson, et al., Les Ondes de Detonation (Editions due Centre National de la Recherche Scientifique, Paris, 1962).
14. R. A. Graham and G. E. Ingram, J. Appl. Phys. 43, 826 (1972).
15. R. A. Graham, Phys. Rev. B., 6, 4779 (1972).
16. R. A. Graham, J. Appl. Phys. 46, 1901 (1975).

17. R. N. Thurston, in Handbuch Der Physik, Ed. S. Flugge (Springer-Verlag, Berlin, 1974).
18. R. A. Graham, J. Appl. Phys. 48, 2153 (1977).
19. F. Borgnis, Phys. Rev. 98, 1000 (1955).
20. R.F.S. Hearmon, An Introduction to Applied Anisotropic Elasticity (Oxford University Press, London, 1961).
21. K. Brugger, J. Appl. Phys. 36, 759 (1961).
22. J. N. Johnson, J. Appl. Phys. 42, 5522 (1971).
23. Proceedings of the I.R.E. 14, 1378 (1949).
24. A. W. Warner, M. Onoe, and G. A. Coquin, J. Acoust. Soc. Amer. 42, 1223 (1967).
25. R. T. Smith and F. S. Walsh, J. Appl. Phys. 42, 2219 (1979).
26. In this configuration the gage is directly impacted by a flyer plate thereby avoiding the complexity of the specimen gage interaction.
27. L. M. Barker and R. E. Hollenbach, J. Appl. Phys. 41, 4208 (1970).
28. This ratio is for d-values.

## Appendix A

### OPERATION MODES FOR PIEZOELECTRIC GAGES\*

Piezoelectric gages may be used in either of two modes: current (or short circuit) mode and charge (or open circuit) mode. The current mode is used for stress measurements for time durations less than the transit time through the gage ( $\sim \mu\text{s}$  time scales). The charge mode is used for stress measurements for time durations ( $\sim \text{ms}$  time scales) much greater than transit time through the gage. This appendix presents the electrical equations for each of these modes to show the similarity in the basic piezoelectric concepts for gage design. The assumptions used in deriving these relations are similar to those used by Graham et al.<sup>5</sup>

Assuming that the electric fields are linear and one-dimensional, we have

$$D(h,t) = \underline{\epsilon}(h,t) \cdot E(h,t) + P(h,t) \quad (\text{A.1})$$

where  $D$  = Displacement field

$\underline{\epsilon}$  = Dielectric permittivity<sup>†</sup>

$E$  = Electric field

$P$  = Polarization field

$h$  = Spatial coordinate through the thickness of the material.

If we assume constant permittivity, we can write

$$\int_0^l D \cdot dh = \underline{\epsilon} \int_0^l E \cdot dh + \int_0^l P \cdot dh \quad (\text{A.2})$$

\* Parts of the material presented here are taken from a review by Y. M. Gupta, "Response and Use of a Quartz Gage," Shock Dynamics Laboratory Internal Report 73-03, Washington State University (1973).

† To avoid confusion with the symbol used for strains, we denote permittivity with a bar below the symbol.

where  $\ell$  = gage thickness. The assumption of zero conductivity in the gage gives

$$\nabla \cdot \vec{D} = \partial D / \partial h = 0$$

Putting this expression into Eq. (A.2), we have

$$D = \frac{1}{\ell} \left[ \underline{\epsilon} \int_0^{\ell} E \cdot dh + \int_0^{\ell} P \cdot dh \right] \quad (A.3)$$

Current flow,  $i$ , between the gage faces may be expressed using Maxwell's equations

$$i = \frac{dq}{dt} = \frac{d}{dt} \int \left[ \nabla \cdot \vec{D} \right] dv = A \cdot \frac{dD}{dt} \quad (A.4)$$

where  $q$  = true charge density

$A$  = area over which the measurements are made.

Eq. (A.4) is now analyzed with respect to the current and charge mode usage.

Current Mode:

The short circuit condition between the gage faces gives

$$\int_0^{\ell} E \cdot dh = 0 \quad (A.5)$$

Combining Eqs. (A.3), (A.4), and (A.5), we have

$$i = \frac{A}{\ell} \frac{d}{dt} \int_0^{\ell} P \cdot dh \quad (A.6)$$

If we assume that  $P = f\sigma$ , where  $\sigma$  is the stress component of interest and  $f$  is the appropriate piezoelectric constant,\* we have

---

\* This scalar relationship is only possible if the piezoelectric tensor has the appropriate form. Details of relating polarization fields to stresses is the subject of Section III.C.

$$i = \frac{\Delta f}{\ell} \frac{d}{dt} \int_0^{\ell} \sigma dh \quad (\text{A.7})$$

Because the gage itself is assumed to be linear elastic, we can write

$$\sigma(h,t) = \sigma(h - U \cdot t) \quad (\text{A.8})$$

where  $U$  is wave velocity in the gage. Putting Eq. (A.8) in (A.7) and recognizing that  $h$  and  $t$  are independent variables, we obtain

$$i = - \frac{fAU}{\ell} \{ \sigma(\ell) - \sigma(0) \} \quad (\text{A.9})$$

Equation (A.9) is the fundamental equation for this mode and relates the current output to stress difference between the two faces of the gage. For times less than the transit through the gage,  $\sigma(\ell) = 0$  in Eq. (A.9).

#### Charge Mode:

The open circuit condition between the gage faces is expressed by setting  $i = 0$  in Eq. (A.4). This gives

$$\frac{d}{dt} \left[ \epsilon \int_0^{\ell} E dh + \int_0^{\ell} P dh \right] = 0 \quad (\text{A.10})$$

Substituting the following definitions of voltage and permittivity

$$V = - \int_0^{\ell} E dh \quad \text{and} \quad \underline{\epsilon} = \frac{\ell c}{A} \quad (\text{A.11})$$

where  $c$  = capacitance, in Eq. (A.10), we have

$$V = \frac{A}{\ell c} \int_0^{\ell} P \cdot dh \quad (\text{A.12})$$

Assuming  $P = f\sigma$  as before, we can write

$$V = \frac{f\Lambda}{c} \left[ \frac{1}{\ell} \int_0^{\ell} \sigma dh \right] \quad (\text{A.13})$$

The term in the brackets is the average stress  $\sigma_{av}$  through the gage thickness.

$$V = \frac{f\Lambda\sigma_{av}}{c} \quad (\text{A.14})$$

Equation (A.14) is the fundamental equation for this mode and relates the voltage output to the average stress in the piezoelectric gage.

Equations (A.9) and (A.14) show that both modes of operation use the same piezoelectric relation  $P = f\sigma$ . Hence, the piezoelectric developments from our impact work (using the current mode) are directly applicable to the design of field gages that would use the charge mode.

## Appendix B

### TRANSFORMATION OF PIEZOELECTRIC CONSTANTS

This appendix describes a simple and convenient method to determine the crystallographic orientations best suited for piezoelectric gage applications. Although considerable information exists on piezoelectric constants along particular directions, the method presented is more general and convenient for the applications of interest.

The third-rank piezoelectric tensors defined in Section III can be transformed as follows

$$e'_{ijk} = a_{ip} a_{jq} a_{kr} e_{pqr} \quad (\text{B.1})$$

$$d'_{ijk} = a_{il} a_{jm} a_{kn} d_{lmn}, \quad (\text{B.2})$$

where  $a_{mn}$  is the transformation matrix given by Eq. (2) in Section II. In defining the coordinate rotations for our work, we have chosen the Institute of Radio Engineers (IRE) conventions, instead of the usual solid angles. We have numerically solved equations (B.1) and (B.2) for coordinate rotations between  $0^\circ$  and  $180^\circ$  (in increments of  $1^\circ$ ) about the X, Y, or Z axes. The numerical program has the following inputs.

- (1) Reading in the axis of rotation, that is, 1 or 2 or 3  
(Corresponding to X or Y or Z).
- (2) Reading in the crystal type and the piezoelectric matrix  
(numerical values) in the crystallographic system.

The above input is used to determine the rotated constants as follows

- (1) Change the piezoelectric constants from the matrix to tensor notation.
- (2) Construct the transformation matrices for the rotation angle.
- (3) Transform the piezoelectric tensor.

- (4) Convert the transformed tensor back to the matrix form.
- (5) Print out the angle of rotation and the transformed piezoelectric matrix.
- (6) Repeat the above steps for all desired angles.

The differences in converting e and d values from matrices to tensors and vice-versa are included.

As an example of this procedure, we show the piezoelectric stress matrix ( $e_{ij}$ 's) for  $\text{LiNbO}_3$  rotated about the X-axis in Table B.1. The values shown are for rotation angles between  $0^\circ$  to  $19^\circ$  and  $152^\circ$  to  $173^\circ$ . The non-zero strains in the impact experiments are  $\epsilon_2'$  and  $\epsilon_4'$ . From the matrices in Table B.1 one can easily determine the usefulness of a particular orientation. Note the marked change in shear-to-compression sensitivity ratio ( $e_{24}'/e_{22}'$ ) in going from  $162^\circ$  to  $164^\circ$ .



Table B.1 (Concluded)

TRANSFORMED VALUES

152 DEGREE	0.	0.	0.	-2.179E+00	3.911E+00	153 DEGREE	0.	0.	0.	-2.247E+00	3.872E+00
2.254E+00	1.350E+00	-2.543E+00	-3.051E+00	0.	0.	2.270E+00	1.243E+00	-2.486E+00	-3.133E+00	0.	0.
9.377E-01	6.544E-02	-2.999E+00	-8.854E-01	0.	0.	8.198E-01	1.192E-02	-2.924E+00	-8.837E-01	0.	0.
154 DEGREE	0.	0.	0.	-2.314E+00	3.832E+00	155 DEGREE	0.	0.	0.	-2.381E+00	3.791E+00
2.285E+00	1.132E+00	-2.426E+00	-3.212E+00	0.	0.	2.300E+00	1.017E+00	-2.362E+00	-3.288E+00	0.	0.
8.585E-01	-3.957E-02	-2.850E+00	-8.785E-01	0.	0.	8.185E-01	-8.885E-02	-2.778E+00	-8.698E-01	0.	0.
156 DEGREE	0.	0.	0.	-2.447E+00	3.749E+00	157 DEGREE	0.	0.	0.	-2.512E+00	3.706E+00
2.313E+00	8.992E-01	-2.293E+00	-3.361E+00	0.	0.	2.327E+00	7.799E-01	-2.222E+00	-3.429E+00	0.	0.
7.789E-01	-1.357E-01	-2.707E+00	-8.576E-01	0.	0.	7.378E-01	-1.801E-01	-2.638E+00	-8.423E-01	0.	0.
158 DEGREE	0.	0.	0.	-2.576E+00	3.662E+00	159 DEGREE	0.	0.	0.	-2.639E+00	3.616E+00
2.339E+00	6.532E-01	-2.146E+00	-3.495E+00	0.	0.	2.351E+00	5.263E-01	-2.067E+00	-3.556E+00	0.	0.
6.979E-01	-2.218E-01	-2.571E+00	-8.238E-01	0.	0.	6.561E-01	-2.603E-01	-2.506E+00	-8.023E-01	0.	0.
160 DEGREE	0.	0.	0.	-2.702E+00	3.569E+00	161 DEGREE	0.	0.	0.	-2.764E+00	3.522E+00
2.362E+00	3.963E-01	-1.985E+00	-3.613E+00	0.	0.	2.372E+00	2.638E-01	-1.900E+00	-3.466E+00	0.	0.
6.159E-01	-2.960E-01	-2.443E+00	-7.781E-01	0.	0.	5.737E-01	-3.284E-01	-2.382E+00	-7.512E-01	0.	0.
162 DEGREE	0.	0.	0.	-2.825E+00	3.473E+00	163 DEGREE	0.	0.	0.	-2.885E+00	3.423E+00
2.382E+00	1.289E-01	-1.813E+00	-3.715E+00	0.	0.	2.391E+00	-8.001E-03	-1.722E+00	-3.759E+00	0.	0.
5.322E-01	-3.578E-01	-2.324E+00	-7.219E-01	0.	0.	4.905E-01	-3.833E-01	-2.268E+00	-6.902E-01	0.	0.
164 DEGREE	0.	0.	0.	-2.945E+00	3.372E+00	165 DEGREE	0.	0.	0.	-3.003E+00	3.320E+00
2.399E+00	1.468E-01	-1.630E+00	-3.799E+00	0.	0.	2.407E+00	-2.873E-01	-1.533E+00	-3.834E+00	0.	0.
4.487E-01	-4.055E-01	-2.216E+00	-6.565E-01	0.	0.	4.068E-01	-4.240E-01	-2.166E+00	-6.209E-01	0.	0.
166 DEGREE	0.	0.	0.	-3.060E+00	3.267E+00	167 DEGREE	0.	0.	0.	-3.117E+00	3.214E+00
2.413E+00	4.292E-01	-1.438E+00	-3.864E+00	0.	0.	2.419E+00	-5.723E-01	-1.339E+00	-3.889E+00	0.	0.
3.647E-01	-4.387E-01	-2.119E+00	-5.836E-01	0.	0.	3.225E-01	-4.497E-01	-2.075E+00	-5.447E-01	0.	0.
168 DEGREE	0.	0.	0.	-3.173E+00	3.159E+00	169 DEGREE	0.	0.	0.	-3.227E+00	3.103E+00
2.425E+00	7.163E-01	-1.239E+00	-3.910E+00	0.	0.	2.429E+00	-8.611E-01	-1.137E+00	-3.925E+00	0.	0.
2.803E-01	-4.568E-01	-2.034E+00	-5.046E-01	0.	0.	2.379E-01	-4.599E-01	-1.996E+00	-4.634E-01	0.	0.
170 DEGREE	0.	0.	0.	-3.281E+00	3.046E+00	171 DEGREE	0.	0.	0.	-3.334E+00	2.988E+00
2.433E+00	1.008E+00	-1.034E+00	-3.935E+00	0.	0.	2.436E+00	-1.152E+00	-9.303E-01	-3.941E+00	0.	0.
1.955E-01	-4.591E-01	-1.962E+00	-4.213E-01	0.	0.	1.530E-01	-4.542E-01	-1.931E+00	-3.785E-01	0.	0.
172 DEGREE	0.	0.	0.	-3.385E+00	2.930E+00	173 DEGREE	0.	0.	0.	-3.436E+00	2.870E+00
2.438E+00	1.291E+00	-8.266E-01	-3.941E+00	0.	0.	2.440E+00	-1.442E+00	-7.221E-01	-3.936E+00	0.	0.
1.104E-01	-4.453E-01	-1.903E+00	-3.354E-01	0.	0.	6.786E-02	-4.323E-01	-1.879E+00	-2.919E-01	0.	0.

## DISTRIBUTION LIST

### DEPARTMENT OF DEFENSE

Assistant to the Secretary of Defense  
Atomic Energy  
ATTN: Executive Assistant

Defense Advanced Rsch. Proj. Agency  
ATTN: TIO

Defense Intelligence Agency  
2 cy ATTN: DB-4N

Defense Nuclear Agency  
ATTN: DDST  
2 cy ATTN: SPSS  
4 cy ATTN: TITL

Defense Technical Information Center  
12 cy ATTN: DD

Federal Emergency Management Agency  
ATTN: Hazard Eval. & Vul. Red. Div.,  
G. Sisson

Field Command  
Defense Nuclear Agency  
ATTN: FCPR  
ATTN: FCPR, J. Hill

Field Command  
Defense Nuclear Agency  
Livermore Division  
ATTN: FCPRL

Interservice Nuclear Weapons School  
ATTN: TTV

Joint Strat. Tgt. Planning Staff  
ATTN: NRI-STINFO Library

Undersecretary of Defense for Rsch. & Engrg.  
ATTN: Strategic & Space Systems (OS)

NATO School (SHAPE)  
ATTN: U.S. Documents Officer

DEPARTMENT OF THE ARMY

Deputy Chief of Staff for Ops. & Plans  
Department of the Army  
ATTN: MOCA-ADL

Harry Diamond Laboratories  
Department of the Army  
ATTN: DELHD-N-P  
ATTN: DELHD-I-TL

U.S. Army Ballistic Research Labs  
ATTN: DRDAR-TSB-S

U.S. Army Communications Cmd.  
ATTN: Technical Reference Division

U.S. Army Engineer Waterways Experiment Station  
ATTN: Library  
ATTN: J. Ingram

### DEPARTMENT OF THE ARMY (Continued)

U.S. Army Material & Mechanics Rsch. Ctr.  
ATTN: Technical Library

U.S. Army Materiel Dev. & Readiness Cmd.  
ATTN: DRXAM-TL

U.S. Army Missile Command  
ATTN: RSIC

U.S. Army Mobility Equip. R&D Cmd.  
ATTN: DRDME-WC

U.S. Army Nuclear & Chemical Agency  
ATTN: Library

U.S. Army War College  
ATTN: Library

DEPARTMENT OF THE NAVY

Naval Research Laboratory  
ATTN: Code 2627

Naval Sea Systems Command  
ATTN: SEA-09G53

Naval Surface Weapons Center  
ATTN: Code F31

Naval Weapons Center  
ATTN: Code 233

Naval weapons Evaluation Facility  
ATTN: Code 10

Strategic Systems Project Office  
Department of the Navy  
ATTN: NSP-43

Naval Ship Engineering Center  
ATTN: Code 09G3

Naval Surface Weapons Center  
ATTN: Tech. Lib. & Info Svcs. Branch

Office of Naval Research  
ATTN: Code 715

David Taylor Naval Ship R&D Ctr.  
ATTN: Code L42-3

Naval Construction Battalion Ctr.  
Civil Engineering Laboratory  
ATTN: Code LO8A

Naval Facilities Engineering Cmd.  
ATTN: Code 09M22C

Naval Postgraduate School  
ATTN: Code 0142

DEPARTMENT OF THE AIR FORCE

Air Force Institute of Technology  
ATTN: Library

Air Force Weapons Laboratory, AFSC  
ATTN: SUL  
2 cy ATTN: DED

Assistant Chief of Staff  
Intelligence  
Department of the Air Force  
ATTN: INT

Strategic Air Command  
Department of the Air Force  
ATTN: NRI-STINFO Library

Rome Air Development Center  
Air Force Systems Command  
ATTN: TSLD

DEPARTMENT OF ENERGY

Department of Energy  
Albuquerque Operations Office  
ATTN: CTID

Department of Energy  
Nevada Operations Office  
ATTN: Mail & Records for Technical Library

DEPARTMENT OF ENERGY CONTRACTORS

Lawrence Livermore Laboratory  
ATTN: Document Control for Tech. Info.  
Dept. Library

Sandia Laboratories  
Livermore Laboratory  
ATTN: Document Control for Lib. & Sec.  
Class. Div.

Sandia Laboratories  
ATTN: Document Control for 3141

OTHER GOVERNMENT AGENCY

Department of the Interior  
Bureau of Mines  
ATTN: Technical Library

DEPARTMENT OF DEFENSE CONTRACTORS

Aerospace Corp.  
ATTN: Technical Operations Services

AVCO Research & Systems Group  
ATTN: Library A830

BDM Corp.  
ATTN: Corporate Library

DEPARTMENT OF DEFENSE CONTRACTORS (Continued)

Boeing Co.  
ATTN: Aerospace Library

Calspan Corp.  
ATTN: Library

EG&G Washington Analytical Services Center, Inc.  
ATTN: Library

General Electric Company-TEMPO  
ATTN: DASIAC

IIT Research Institute  
ATTN: Documents Library

Institute for Defense Analyses  
ATTN: Classified Library

Kaman AviDyne  
ATTN: Library

Kaman Sciences Corp.  
ATTN: Library

Lockheed Missiles & Space Co., Inc.  
ATTN: Technical Information Center

Lockheed Missiles & Space Co., Inc.  
ATTN: TIC, Library

Merritt CASES, Inc.  
ATTN: Library

Pacifica Technology  
ATTN: J. Kent

Physics International Co.  
ATTN: Technical Library

R & D Associates  
ATTN: C. MacDonald  
ATTN: Technical Information Center

Science Applications, Inc.  
ATTN: Technical Library

SRI International  
ATTN: Y. Gupta  
ATTN: W. Murri

Systems, Science & Software, Inc.  
ATTN: Library

Terra Tek, Inc.  
ATTN: Library

Tetra Tech, Inc.  
ATTN: Library

TRW Defense & Space Sys. Group  
ATTN: Technical Information Center

Weidlinger Associates, Consulting Engineers  
ATTN: D. Ranlet